Acta Cryst. (1978). A**34**, 667–681

The Short-Range-Order Structure of α-Phase Cu–Al Alloys

BY J. E. EPPERSON, P. FÜRNROHR AND C. ORTIZ*

Max-Planck-Institut für Metallforschung, Institut für Werkstoffwissenschaften, and Institut für Metallkunde der Universität Stuttgart, Stuttgart, Federal Republic of Germany

(*Received* 28 *November* 1977; *accepted* 29 *March* 1978)

A three-dimensional X-ray diffuse scattering investigation of the short-range order in α-phase Cu–Al alloys, and its dependence on alloy composition, quenching temperature and isothermal annealing at 250°C, has been carried out. The Cowley–Warren order coefficients were determined after separation of the size effects using a procedure based on the Borie–Sparks quadratic approximation of atomic displacements. These short-range-order coefficients were analyzed in terms of the complete spectrum of nearest-neighbor atomic configurations, without the necessity of invoking a specific model for the characteristic feature(s) of the local-order structure. Although in the composition range investigated the equilibrium condition is a short-range-ordered structure, the *nearest-neighbor configurations* bear a marked resemblance to the long-period anti-phase-shift structures which have been found in alloys with more Al. Because essentially all of the most highly ordered configurations were found to exist isolated from each other in a 9·13 at.% Al alloy, it is concluded that they represent inherently stable, spatial arrangements of the atoms. In alloys containing 13·56 and 14·76 at.% Al, connected ordered configurations, or small ordered domains, were detected, and this effect increases markedly with increasing Al content. Isothermal annealing at 250°C of a Cu–14·76 at.% Al alloy quenched from 650°C results in a net disordering process; however, superimposed on this, in the early stages of annealing, is an enhancement of the population density of an atomic configuration confined to planes of the {111} type. This is interpreted as evidence for occurrence of the Suzuki mechanism. It is argued that the body of published experimental observations on this alloy system is better understood if one recognizes the existence of stacking faults, and their interaction with the matrix, in addition to that of short-range order.

Introduction

There has been continuing interest in the local-order structure of the α-phase Cu–Al alloys since the electrical resistivity studies on neutron-irradiated material by Wechsler & Kernohan (1958) indicated that a composition-dependent, diffusion-controlled, solid-state reaction occurs under certain conditions. In essence, they concluded that at temperatures below about 200°C slow-cooled alloys exist in a non-equilibrium state and that lattice imperfections introduced by neutron irradiation aid the system in approaching thermodynamic equilibrium. However, their resistivity measurements did not permit the nature of this solid-state reaction to be determined.

X-ray diffraction studies by Houska & Averbach (1959) on powders and two-dimensional studies by Borie & Sparks (1964) on single crystals established conclusively the existence of short-range order (SRO). In the latter work, based on considerations of the symmetry of the scattering diagram and on the positions of the diffuse SRO maxima relative to the superstructure positions, it was suspected that a domain structure existed, the size of the domains being so small that the atomic configurations at the anti-phase boundary were the most characteristic of the alloy. The configuration proposed was made up of four Al atoms arranged tetrahedrally about a Cu atom. They reported that a random distribution of these tetrahedra, constrained so as to prohibit the occurrence of first-nearest-neighbor Al–Al pairs, would yield a set of two-dimensional order parameters in satisfactory, qualitative agreement with the measured values, thus establishing the reasonableness of the tetrahedron model.

Short-range order is not the only type of structural defect known to exist in these α-phase Cu–Al alloys. Howie & Swann (1961) showed that the specific intrinsic stacking-fault energy, γ, is highly dependent on the alloy composition, decreasing rapidly from the value for pure Cu to a low value at about 10 at.% Al, beyond which there is relatively little further change. Hot-stage transmission electron microscopy (TEM) by Hasegawa, Asou & Karashima (1974) on alloys in this latter region showed that the stacking-fault energy is nearly constant below about 200°C and that above this temperature γ increases markedly with temperature. Furthermore, these changes in γ were found to be reversible with temperature, a result that is consistent with the TEM work on long-time aged and quenched specimens by Tisone, Brittain & Meshii (1968).

* Present address: Instituto de Optica, Madrid, Spain.

A composition-dependent stacking-fault energy implies a chemical interaction between the faults and solute atoms (Suzuki, 1952), and there have been several experimental attempts either to determine if segregation of Al to dislocations or stacking faults occurs or which have implicitly assumed this behavior. In addition to the TEM already cited, the small-angle X-ray scattering work by Cahn & Davies (1960), the TEM plus divergent X-ray beam studies by Nakajima, Slade & Weissman (1965), and some small-angle neutron scattering measurements by Epperson, Kostorz, Ortiz and Fürnrohr (1978) have *suggested* that some such reaction is taking place. In each of the latter three cases, the measured effect was small and need not be attributed exclusively to segregation of the solute. It would surely be fair to observe that, although there are sound theoretical grounds for expecting an interaction of the solute atoms with linear and/or planar defects, the results to date are suggestive rather than definitive.

In addition, other explanations based on either bulk segregation or formation of domain structures have been advanced. Based on diffuse X-ray scattering measurements from deliberately abraded polycrystalline bulk samples, Iveronova, Katsnelson & Revkevich (1968) obtained a first-shell order coefficient outside the theoretical limits and concluded that this could be explained by the development of regions alternately enriched in and depleted of Al and to changes in the degree of order within the segregated regions. Trieb, Siebinger & Aubauer (1973) measured the rate of change of electrical resistivity following small, sudden temperature excursions in the range from 200 to 250°C and have proposed that the slower 'ordering' rate, compared to 'disordering' at a given temperature, can be explained on the basis of diffusion-controlled nucleation and growth of ordered particles in a disordered matrix. Recently an extensive work by Gaudig (1975) and by Gaudig & Warlimont (1969, 1978) based experimentally on electrical resistivity, electron microscopy, and differential thermal measurements, as well as on a model fitting of the Borie–Sparks diffuse X-ray scattering data, led also to the conclusion that a domain structure was involved. In their earlier paper, it was thought that the structure was of the particle model variant type; *i.e.* ordered particles in a disordered matrix. However, in the latter work (Gaudig & Warlimont, 1978) it was concluded that the SRO in the α-phase Cu–Al alloys could best be characterized by a microdomain model. The domains were thought to be 10–20 Å in size and separated by diffuse boundaries enriched in one constituent. Within the domains, the order was assumed to be a two-dimensional antiphase-shift structure produced by suitable insertion of antiphase boundaries on the {100} planes.

Thus one sees that while this alloy system has been rather intensively investigated for twenty years, no fully acceptable explanation of the local-order structure has evolved. Since the diffuse diffraction work by Houska & Averbach and by Borie & Sparks cited above, advances in the analytic techniques have been made. A better method is now available (Borie & Sparks, 1971) for separating the size effects from the order component of the diffuse scattering. A real-space representation of the atomic order structure can be reproduced from the measured Cowley–Warren order coefficients (Gehlen & Cohen, 1965) with a considerable degree of confidence (Clapp, 1971), and from this structure the entire spectrum of first-nearest-neighbor atomic configurations can be determined routinely as well as some additional information about how these units are joined together in the first and second coordination shells (Epperson, 1978). The principal purpose of this publication is to report the results of an X-ray diffuse scattering investigation of the α-phase Cu-Al alloys based on the procedures just mentioned in an attempt to characterize the SRO structure more fully and to investigate the systematic changes occurring when an alloy is disordered during isothermal annealing at 250°C.

Experimental procedure

Using a modified Bridgman technique, large Cu–Al single-crystal rods of several compositions ranging from about 4 to 15 at.% Al were grown in graphite crucibles under a protective atmosphere of purified argon in a high-frequency induction furnace. The starting materials were 99·998% Cu and 99·999% Al. After the rods had been homogenized for two days at 700°C, disc-shaped single-crystal samples, 20 mm in diameter, about 3 mm thick and having [520] surface normals, were prepared by spark machining. The worked surface layer was removed by standard mechanical polishing procedures and by etching in concentrated nitric acid. Before each diffraction run, the sample was electropolished for 15 min at −30°C in a stirred bath consisting of two volume parts methanol and one part nitric acid, with a potential of nine volts. The electropolishing procedure removed a layer of about 0·05 mm from the surface. Heat treatments at 400°C or above were done in flowing hydrogen, and, other than when exceptions are stated, the samples were quenched into water at room temperature. Unless otherwise noted, heat treatments at 350°C or below for less than half an hour were done in an oil bath, and those for longer times were carried out in vacuum.

For the samples that were investigated quantitatively by the diffuse-scattering technique, the composition was determined by wet analysis, after completion of the diffraction measurements, of sections cut from the diffraction samples themselves. For qualitative measurements, the composition was ascertained by

comparing the lattice constant with an experimentally determined curve. The absorption constant was also determined from material from the actual samples.

The diffuse X-ray scattering measurements were made with parallel geometry at room temperature on a partially atutomated Siemens diffractometer equipped with an evacuated sample chamber mounted on an Eulerean cradle. A Warren (1954)–Chipman (1956) type doubly bent LiF monochromator* was used in the incident beam to select the Co $K\alpha$ radiation. The detecting system consisted of an Ortec Si(Li) solid-state counter, and associated electronic equipment, with an overall energy resolution of about 200 eV. This resolution permitted the Cu fluorescence radiation, and other wavelength-dependent parasitic effects outside this 200 eV range, to be discriminated electronically from the Co $K\alpha$. The measured diffuse intensity values were converted to absolute units by comparison with the scattering from polystyrene.

A series of one- and two-dimensional measurements to obtain a survey of the changes that can be produced by alloy composition and heat treatment in the α phase Cu–Al alloys were made in the $h_3 = 0$ plane of reciprocal space. For the cases to be analyzed quantitatively, the diffuse scattering was measured throughout the reciprocal space volume shown in Fig. 1. For each such set of measurements, 1671 positions were sampled on an equally spaced rectangular grid in the volume shown. Typically for the Cu–14·76 at.% Al alloy, of the order of 12 000 counts were measured for a point at a diffuse maximum and about 3000 counts in the background region. The analytical procedures used will be outlined in the following section.

Pertinent diffraction theory and analytical procedure

(a) *Diffraction theory*

In the kinematic approximation, the total coherently scattered intensity in electron units, I_{eu}, at a given position in reciprocal space is given by

$$I_{eu}(\mathbf{k}) = \sum_p \sum_q f_p f_q \exp(i\mathbf{k}.\mathbf{R}_{pq}); \qquad (1)$$

here f_p and f_q are the scattering factors of the atoms at sites p and q, respectively, $\mathbf{k}$ is 2π times the diffraction vector, and $\mathbf{R}_{pq}$ is the interatomic vector. In the usual case of alloys where the atoms are not located precisely at the lattice sites, $|\mathbf{R}_{pq}|$ is not required to be constant for a given coordination shell about each atom in the sample. This can be accounted for by incorporating a general displacement term in the interatomic vector and taking the average lattice sites as points of reference. To a second-order approximation of the atomic displacements from the average lattice sites in binary f.c.c. or b.c.c. alloys (Borie & Sparks, 1971), the coherently scattered diffuse intensity can be expressed as

$$\begin{aligned} I(h_1, h_2, h_3) &= NX_A X_B (f_A - f_B)^2 \\ &\times \sum_l \sum_m \sum_n \alpha_{lmn} \cos 2\pi h_1 l \cos 2\pi h_2 m \cos 2\pi h_3 n \\ &- NX_A X_B (f_A - f_B)^2 \sum_l \sum_m \sum_n [h_1 \gamma^x_{lmn} \sin 2\pi h_1 l \\ &\times \cos 2\pi h_2 m \cos 2\pi h_3 n + h_2 \gamma^y_{lmn} \cos 2\pi h_1 l \sin 2\pi h_2 m \\ &\times \cos 2\pi h_3 n + h_3 \gamma^z_{lmn} \cos 2\pi h_1 l \cos 2\pi h_2 m \sin 2\pi h_3 n] \\ &- 4\pi^2 N \sum_l \sum_m \sum_n [h_1^2 \langle \delta^2 \rangle^x_{lmn} + h_2^2 \langle \delta^2 \rangle^y_{lmn} + h_3^2 \langle \delta^2 \rangle^z_{lmn}] \\ &\times \cos 2\pi h_1 l \cos 2\pi h_2 m \cos 2\pi h_3 n + 8\pi^2 N \\ &\times \sum_l \sum_m \sum_n [h_1 h_2 \langle \delta^2 \rangle^{xy}_{lmn} \sin 2\pi h_1 l \sin 2\pi h_2 m \cos 2\pi h_3 n \\ &+ h_1 h_3 \langle \delta^2 \rangle^{xz}_{lmn} \sin 2\pi h_1 l \cos 2\pi h_2 m \sin 2\pi h_3 n \\ &+ h_2 h_3 \langle \delta^2 \rangle^{yz}_{lmn} \cos 2\pi h_1 l \sin 2\pi h_2 m \sin 2\pi h_3 n]. \qquad (2) \end{aligned}$$

X_A and X_B are the atom fractions of species A and B respectively, and N is the number of atoms irradiated. Relative to an arbitrarily chosen origin, the average interatomic vector is given by

$$\langle \mathbf{R}_{lmn} \rangle = l \frac{\mathbf{a}_1}{2} + m \frac{\mathbf{a}_2}{2} + n \frac{\mathbf{a}_3}{2}, \qquad (3)$$

where l, m, and n denote a triplet of integers which specifies a lattice site in relation to the arbitrary origin and $\mathbf{a}_1$, $\mathbf{a}_2$, and $\mathbf{a}_3$, are translation vectors of the cubic unit cell. The continuous variables in reciprocal space, h_1, h_2, and h_3, are related to the diffraction vector by the relationship

$$\left(\frac{\hat{s} - \hat{s}_0}{\lambda}\right) = h_1 \mathbf{b}_1 + h_2 \mathbf{b}_2 + h_3 \mathbf{b}_3, \qquad (4)$$

where $\mathbf{b}_1$, $\mathbf{b}_2$, and $\mathbf{b}_3$ are vectors reciprocal to $\mathbf{a}_1/2$, $\mathbf{a}_2/2$, and $\mathbf{a}_3/2$, respectively, λ is the wavelength, and $\hat{s}$ and $\hat{s}_0$ are unit vectors in the direction of the scattered and

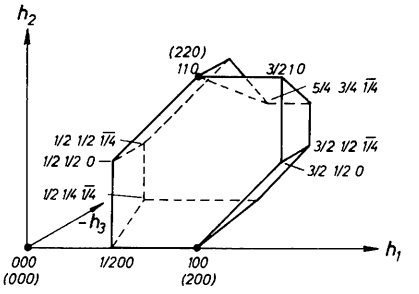

Fig. 1. The region in reciprocal space in which intensity measurements were made for the three-dimensional diffuse-scattering investigation.

* The doubly bent LiF monochromator, as well as a piece of polystyrene, was loaned to us by Dr C. J. Sparks Jr.

incident beams respectively. The Cowley–Warren order coefficients (Cowley, 1950) are defined as

$$\alpha_{lmn} = 1 - \frac{p^{A|B}_{lmn}}{X_B}, \qquad (5)$$

where $p^{A|B}_{lmn}$ is the conditional probability of finding a B type atom at site l, m, n relative to an A atom. A detailed consideration of the size-effect parameters, γ^{j}_{lmn}, $\langle\delta^2\rangle^{j}_{lmn}$ and $\langle\delta^2\rangle^{ij}_{lmn}$ $(i \neq j = x,y,z)$, is outside the intended scope of the present work. It is sufficient to note that they are related to the components of the displacement vector. Additional details can be arrived at from considerations to be found in the original paper by Borie & Sparks.

(*b*) *Analytic procedure*

The sets of diffuse scattering data were converted to absolute units (electron units/atom) by comparison with the measured total scattering from amorphous polystyrene at $\sin\theta/\lambda = 0{\cdot}5$ Å^{-1} by using the relationship

$$\frac{I_{eu}}{N} = \left(\frac{I_{eu}}{M}\right)_p \frac{M_s(\mu/\rho)_s P_p}{M_p(\mu/\rho)_p P_s I_p} I_s, \qquad (6)$$

where I_{eu}/M is the theoretical total scattering in electron units per molecule of polystyrene (C_8H_8), M_s and M_p are molecular weights, $(\mu/\rho)_s$ and $(\mu/\rho)_p$ are mass absorption coefficients, P_s and P_p are polarization factors, and I_s and I_p are the measured intensities in counts/time. The subscripts s and p denote sample and polystyrene respectively. A correction for the Compton-modified scattering was computed with the incoherent scattering data from Freeman (1959*a*,*b*). The coherent scattering factors were taken from Doyle & Turner (1968), and the anomalous dispersion was corrected for by using the parameters computed by Cromer (1965). (The values for Cu were actually obtained by interpolation between neighboring values.) Following the procedure of Warren & Mozzi (1966), a correction of 4·48%, due to double scattering, was added to the computed total single scattering for amorphous polystyrene.

It has been assumed that the formalism of the quadratic approximation of the atomic displacements by Borie & Sparks (1971) (B–S) is an adequate representation of the coherently scattered diffuse intensity.* Taking advantage of the fact that the four components of the diffuse scattering, as described by the triple summations in equation (2), have different symmetry in reciprocal space, these terms were separated, in this case by invoking the symmetry appropriate for statistically f.c.c. alloys, and the corresponding order and size-effect coefficients were obtained by Fourier inversion of the individual arrays.

To create an atomic model depicting the local-order arrangements represented by the α_{lmn}, a digital computer program of the type developed originally by Gehlen & Cohen (1965) was written. Starting with an initially nearly random 8000 'atom' f.c.c. matrix having the same composition as the alloy, the array was searched in an unbiased manner for pairs of unlike atoms which could be exchanged so as to improve the agreement with the experimentally determined α_{lmn} being fitted. This searching sequence was based on a randomly chosen non-repeating series of 8000 integers which specified the lattice sites. The search–exchange procedure was continued until the first six α's were in satisfactory agreement. (Both the size of the matrix and the number of α's to be fitted are optional.) The resulting fitted array will henceforth be referred to as the GC structure.

The complete distribution of nearest-neighbor atomic configurations was determined, with no assumptions beyond those required in arriving at the GC structure. In addition, the distribution of configurations in the first and second coordination shells about the 'center' Cu atom of each type of configuration was determined.

Results and discussion

(*a*) *General*

The occurrence of significant short-range order in the α-phase Cu-Al alloys is very dependent on the composition, as is illustrated by the series of isointensity contour maps in Fig. 2. What is shown here is the total scattered intensity, in Laue monotonic units, measured in the $h_3 = 0$ plane of reciprocal space for single-crystal samples of the indicated compositions and heat treatments. For alloys containing much less than around 9 at.% Al, the SRO diffuse scattering is quite weak, and it is doubtful if alloys containing less than about 5 or 6 at.% Al could be analyzed satisfactorily with the diffuse scattering technique. The quantitative work being reported here was done on the alloys containing 9·13, 13·56 and 14·76 at.% Al.

In the raw diffraction patterns shown in Fig. 2, there is considerable distortion due to the fact that the atoms do not lie precisely at the average lattice sites. However, after separation of the size effects, the order diffuse maxima in the $h_3 = 0$ plane are found in the well-known four-leaf-clover pattern, centred on the $L1_2$ superlattice positions (see Fig. 7).

The degree of SRO has a complex dependence on the thermal history, a fact that is most easily demonstrated

* The B–S separation procedure assumes that in a series expansion of the exponential containing the atomic displacements the terms higher in order than the quadratic may be neglected and that the scattering-factor ratios are independent of the length of the scattering vector. The latter is the more limiting assumption, and a recent method by Tibbals (1975) allows a better separation.

by considering the height above background of the diffuse maximum at $(h_1,h_2,h_3) \simeq (0{\cdot}5, 0{\cdot}133, 0{\cdot}0)$ in Fig. 2(*e*).* Fig. 3 shows the diffuse peak intensity for the Cu–14·76 at.% Al alloy *versus* the annealing temperature. All these intensity measurements were made at room temperature. For temperatures of 400°C and above, the samples were annealed one hour in flowing H_2 and quenched to room temperature in water. For temperatures of 340°C and below, the samples were first quenched to room temperature from 650°C and then given a long-time anneal in vacuum at the indicated temperature. The behavior is somewhat unusual in that the degree of SRO goes through a minimum near 350°C and increases with increasing quenching temperature in the range from about 350 to 700°C.

This is an indication that the state of order characteristic of the higher annealing temperatures is not retained upon quenching to room temperature. It is assumed that if the diffuse scattering were measured at temperature a curve of the general form indicated by the dashed line would result. This contention is supported by the heat-capacity measurements by Brooks & Stansbury (1963) and Matsuo & Clarebrough (1963); the latter showed that, on reheating a slow cooled Cu-15 at.% Al alloy, there was a surge of energy absorption in the range from 226 to 290°C and that above 290°C energy was absorbed at a low constant rate. The electrical resistivity measurements by Wechsler & Kernohan (1959) indicate that the position of the minimum shown in Fig. 3 should be sensitive to the effective cooling rate. Thus it is clear that the thermal history of a specimen must be known if changes induced by a given final heat treatment are to be interpreted meaningfully.

Using the procedure for three-dimensional diffuse scattering measurements outlined in the previous section, a more extensive and quantitative analysis has been made for two series of conditions: one series consisted of an investigation of the nature of the short-range order formed in alloys containing 9·13, 13·56,

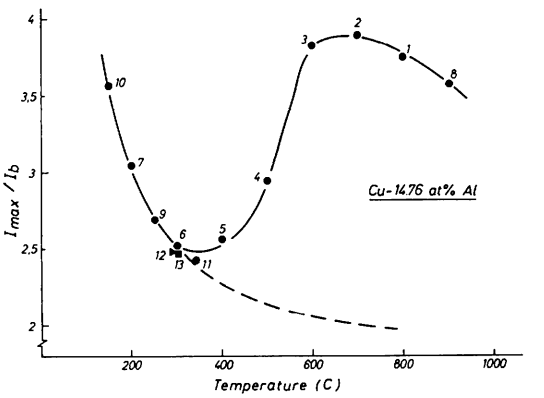

Fig. 3. The ratio of the peak diffuse order intensity at $(h_1,h_2,h_3) \simeq (0{\cdot}5,0{\cdot}133,0{\cdot}0)$ to the background for a Cu–14·76 at.% Al single crystal *vs* annealing temperature. For 400°C and above the sample was annealed 1 h at the indicated temperature in flowing hydrogen and quenched to room temperature in water. For 340°C and below, the sample was quenched from 650°C and given a long-time anneal in vacuum at the indicated temperature. The number indicates the sequence in which the experiments were done.

* The coordinate scale used here is that conveniently employed in diffuse scattering work where, for example, the position of the 200 Bragg reflection is denoted as 1,0,0.

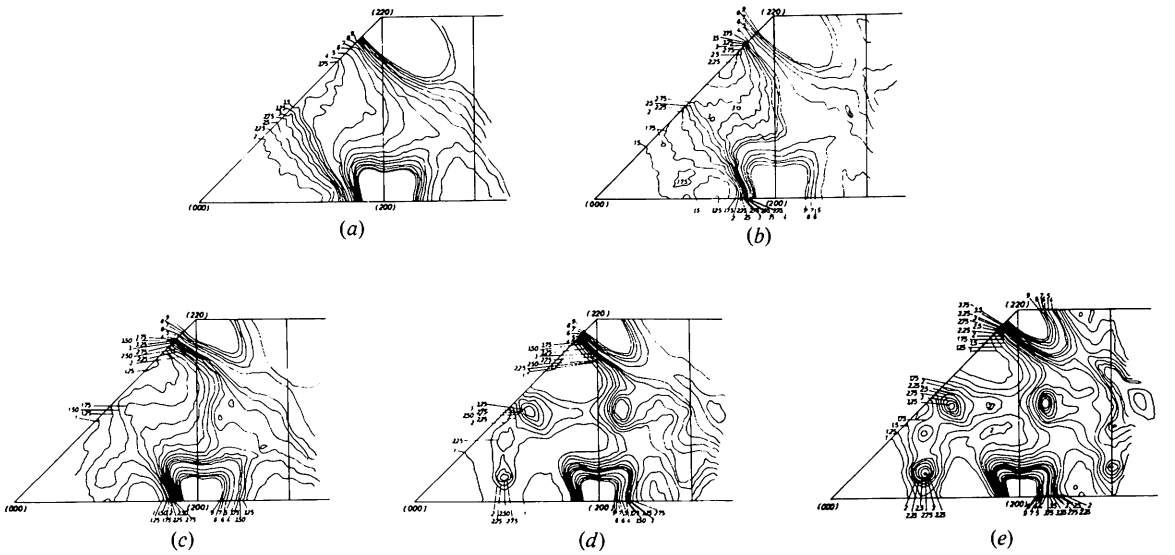

Fig. 2. Isointensity contour diagrams in the $h_3 = 0$ plane of reciprocal space for a series of Cu–Al alloys. Shown here is the total scattering in Laue monotonic units for: (*a*) Cu–4·1 at.% Al; 1 h at 650°C, q. to r.t., 1580 h at 150°C. (*b*) Cu–6·1 at.% Al; 1 h at 650°C, q. to r.t., 1580 h at 150°C. (*c*) Cu–9·13 at.% Al; 1 h at 600°C, q. to r.t., 645 h at 200°C. (*d*) Cu–13·56 at.%; 1 h at 600°C, q. to r.t., 670 h at 200°C. (*e*) Cu–14·76 at.% Al; 1 h at 650°C, q. to r.t., 1580 h at 150°C.

and 14·76 at.% Al upon aging 1580 h at 150°C following quenching from 650°C, and the second series was an investigation of the changes induced in the SRO by isothermal annealing at 250°C of a Cu–14·76 at.% Al alloy single crystal, again after quenching from 650°C.

The experimentally determined Cowley–Warren order coefficients are given in Tables 1 and 2 for the composition-dependent and isothermal measurements respectively. Inasmuch as the criterion used in producing the GC structure is the agreement with the experimental α_{lmn}, the coefficients computed from the modelled 8000-atom GC structure are given so that the quality of fit can be judged. In the absence of sufficient theoretical guidance, a moderately conservative approach has been used in that the first six α_{lmn} were fitted.

Before considering the SRO structure in more detail, a couple of general observations are in order. It will be noted that, except for the 9 at.% Al alloy, the experimental α_{000} parameters are considerably nearer the theoretical value of unity than is customarily obtained, and this agreement can probably be traced to the use of the energy-dispersive detection system.

As can easily be seen from Fig. 2(*c*), the diffuse scattering from the 9 at.% Al alloy is much weaker than that from the other alloys being considered here, and the results, although still statistically significant, are correspondingly less reliable. It will also be noted from Tables 1 and 2 that for the samples aged for long times

Table 1. *Experimental* (Expt.) *and modelled* (Mod.) *Cowley–Warren order coefficients,* α_{lmn}, *for* Cu–Al *alloys containing* 9·13, 13·56, *and* 14·76 at.% Al, *each annealed* 1580 h *at* 150 °C

		α_{lmn}*		α_{lmn}†		α_{lmn}‡	
i	*lmn*	Expt.	Mod.	Expt.	Mod.	Expt.	Mod.
0	000	0·910	1·0000	1·035	1·0000	1·015	1·0000
1	110	−0·109	−0·1006	−0·154	−0·1542	−0·171	−0·1709
2	200	0·079	0·0786	0·093	0·0926	0·125	0·1245
3	211	0·006	0·0057	0·032	0·0316	0·042	0·0416
4	220	−0·002	−0·0022	−0·002	−0·0023	−0·004	−0·0043
5	310	−0·010	−0·0102	−0·024	−0·0242	−0·034	−0·0343
6	222	−0·006	−0·0065	−0·021	−0·0212	−0·032	−0·0324
7	321	0·006	0·0021	0·002	0·0050	0·003	0·0078
8	400	0·005	0·0159	0·005	0·0208	0·021	0·0305
9*a*	330	0·001	0·0126	−0·005	−0·0039	−0·008	0·0026
9*b*	411	−0·004	−0·0032	0·003	0·0036	0·005	0·0040
10	420	−0·001	−0·0033	0·004	0·0080	0·007	−0·0034

* Cu–9·13 at.% Al; α_{110} (min) = −0·1005
† Cu–13·56 at.% Al; α_{110} (min) = −0·1569
‡ Cu–14·76 at.% Al; α_{110} (min) = −0·1732

Table 2. *Experimental* (Expt.) *and modelled* (Mod.) *Cowley–Warren order coefficients,* α_{lmn}, *for a* Cu–14·76 at.% Al *sample isothermally annealed at* 250 °C *as indicated, after quenching from* 650 °C

		α_{lmn}*		α_{lmn}†		α_{lmn}‡		α_{lmn}§	
i	*lmn*	Expt.	Mod.	Expt.	Mod.	Expt.	Mod.	Expt.	Mod.
0	000	1·052	1·0000	1·043	1·0000	1·048	1·0000	0·998	1·0000
1	110	−0·175	−0·1732	−0·166	−0·1656	−0·156	−0·1561	−0·149	−0·1492
2	200	0·127	0·1265	0·098	0·0977	0·091	0·0907	0·083	0·0828
3	211	0·041	0·0406	0·039	0·0386	0·032	0·0317	0·033	0·0326
4	220	−0·002	−0·0023	0·003	0·0026	0·000	−0·0003	−0·002	−0·0023
5	310	−0·033	−0·0333	−0·027	−0·0273	−0·023	−0·0233	−0·021	−0·0213
6	222	−0·033	−0·0277	−0·029	−0·0294	−0·024	−0·0244	−0·022	−0·0222
7	321	0·004	0·0067	0·000	0·0060	0·002	0·0103	0·000	−0·0003
8	400	0·012	0·0195	0·013	0·0172	0·011	0·0175	0·014	0·0020
9*a*	330	−0·014	−0·0048	−0·009	−0·0005	−0·009	−0·0108	−0·005	0·0030
9*b*	411	0·009	0·0088	0·005	0·0062	0·003	0·0033	0·003	0·0122
10	420	0·002	−0·0024	0·010	−0·0011	0·008	−0·0038	0·007	−0·0008

* 1 h at 650 °C in flowing H_2, quenched to room temperature (q. to r.t.) (2 weeks at r.t.)
† 1 h at 650 °C in flowing H_2, q. to r.t., 2·5 min at 250 °C in oil, q. to r.t.
‡ 1 h at 650 °C in flowing H_2, q. to r.t., total of 20 min at 250 °C in oil, q. to r.t.
§ 1 h at 650 °C in flowing H_2, q. to r.t., total of 117 h at 250 °C, q. to r.t.

at 150 °C, the α_{110} values are sensibly equal* to the theoretical lower limit for the given compositions. This is immediate proof that, in such a condition, Al–Al first nearest neighbors are forbidden. Note, however, that this is no longer rigorously true when the 14·76 at.% Al alloy is isothermally annealed at 250 °C and begins to disorder.

In order to obtain more insight about the short-range atomic arrangements in these α-phase Cu–Al alloys, the GC structures have been searched for all possible first-nearest-neighbor configurations. The first 20 species of the resulting spectra of configurations of Al about Cu atoms for the composition-dependent series are given in Table 3, along with those for the corresponding random alloys, and similarly the spectra for the isothermal annealing at 250 °C of the Cu–14·76 at.% Al alloy are given in Table 4. The method for determining the spectra and explanation of the notation are given elsewhere (Epperson, 1978). The short-range-ordered structures are comparatively simple in that no more than 16 of the 144 possible configuration types for Al about Cu atoms are found in the first series (Table 3), and no more than 27 configurations of Al about Cu are found after partially disordering during isothermal annealing at 250 °C.

* An attempt to interpret α_{110} values outside the theoretical lower limit in terms of the atomic arrangement on the lattice sites would require that there be a *negative* number of first nearest-neighbor Al–Al pairs.

Table 3. *Percentage of* Cu *atoms having the indicated configurations in three* Cu–Al *alloys annealed* 1580 h *at* 150 °C *and, for comparison, the corresponding random alloys*

Ci	*P*(*Ci*)*		*P*(*Ci*)†		*P*(*Ci*)‡	
	Expt.	Random	Expt.	Random	Expt.	Random
*C*1	20·88	31·06	3·67	17·37	1·99	14·62
*C*2	44·05	39·44	27·42	32·35	21·19	30·59
*C*3	11·43	3·55	15·24	5·23	15·37	5·02
*C*4	3·04	1·95	5·97	2·83	5·35	2·70
*C*5	14·39	7·70	26·04	10·37	25·81	11·38
*C*6	0·00	7·19	0·32	10·64	0·29	10·09
*C*7	2·05	0·43	5·74	0·75	7·61	0·81
*C*8	3·23	0·95	10·53	1·53	14·97	1·88
*C*9	0·63	0·23	3·38	0·49	4·33	0·67
*C*10	0·00	1·51	0·16	3·47	0·21	3·42
*C*11	0·00	1·47	0·09	3·21	0·19	3·28
*C*12	0·00	0·81	0·14	1·49	0·07	1·86
*C*13	0·00	0·84	0·00	1·36	0·00	2·10
*C*14	0·00	0·72	0·00	1·65	0·00	1·98
*C*15	0·00	0·25	0·00	0·58	0·00	0·81
*C*16	0·15	0·00	0·35	0·01	0·88	0·03
*C*17	0·14	0·00	0·78	0·03	1·67	0·07
*C*18	0·00	0·12	0·09	0·54	0·04	0·84
*C*19	0·00	0·08	0·07	0·49	0·01	0·48
*C*20	0·00	0·15	0·00	0·45	0·00	0·85

* Cu–9·13 at. % Al
† Cu–13·56 at. % Al
‡ Cu–14·76 at. % Al

(*b*) *The nature of the short-range order*

In order to aid in visualizing the short-range-order structure, an example of a proposed sequential relationship between the configurations tabulated here is illustrated in Fig. 4 for the Cu–14·76 at.% Al alloy annealed one hour at 650 °C and quenched to room temperature. This data set was chosen for illustration because the ten configurations were present in all conditions investigated. Additional configurations appear in some cases, but they are few in number and are considered to be of less fundamental significance. The relationship can be understood in terms of two principal chains of the first-nearest-neighbor configurations: one chain derives from an ordered unit consisting of four Al atoms arranged tetrahedrally about a Cu atom and the other from a planar, Cu_3Au-type ring of four Al atoms about a Cu atom. In each case, a single nearest-neighbor jump of an Al atom would suffice to transform a unit to the adjoining configuration, as sketched in Fig. 4. The less ordered species may be considered as 'defect' variants of either *C*16 or *C*17, but the configuration *C*9 appears to play a somewhat

Table 4. *Percentage of* Cu *atoms having the indicated configurations in the* 250 °C *isothermal annealing series for a* Cu–14·76 at. % Al *alloy*

Ci	*P*(*Ci*)*	*P*(*Ci*)†	*P*(*Ci*)‡	*P*(*Ci*)§	*P*(*Ci*)¶
*C*1	1·92	1·79	2·35	2·74	14·62
*C*2	20·19	20·87	21·43	23·08	30·59
*C*3	16·07	13·99	14·36	13·23	5·02
*C*4	5·79	6·38	5·98	5·47	2·70
*C*5	26·51	27·31	25·85	24·48	11·38
*C*6	0·00	0·79	1·55	2·01	10·09
*C*7	7·82	7·26	6·69	6·12	0·81
*C*8	15·13	13·65	12·12	11·57	1·88
*C*9	4·19	4·34	3·86	3·70	0·67
*C*10	0·00	0·67	1·45	1·94	3·42
*C*11	0·00	0·60	1·14	1·75	3·28
*C*12	0·00	0·26	0·66	0·75	1·86
*C*13	0·00	0·01	0·03	0·00	2·10
*C*14	0·00	0·01	0·06	0·07	1·98
*C*15	0·00	0·00	0·00	0·00	0·81
*C*16	0·76	0·59	0·50	0·45	0·03
*C*17	1·60	1·17	1·04	1·03	0·07
*C*18	0·00	0·12	0·34	0·73	0·84
*C*19	0·00	0·16	0·40	0·66	0·48
*C*20	0·00	0·01	0·03	0·03	0·85

* 1 h at 650 °C in flowing H_2, q. to r.t. (2 weeks at r.t.)
† 1 h at 650 °C in flowing H_2, q. to r.t., 2·5 min at 250 °C in oil, q. to r.t.
‡ 1 h at 650 °C in flowing H_2, q. to r.t., total of 20 min at 250 °C in oil, q. to r.t.
§ 1 h at 650 °C in flowing H_2, q. to r.t., total of 117 h at 250 °C, q. to r.t.
¶ Computed random GC structure for a 14·76 at % alloy.

special role. Hence in the following discussion, primary emphasis will be placed on the behavior of configurations $C9$, $C16$, and $C17$ with changes in composition and with selected isothermal annealing.

The composition dependence of these three configurations for alloys quenched from 650°C and annealed 1580 h at 150°C and, for comparison, the corresponding values computed for several random solid-solution alloys and those derived from some published data on a Cu–16 at.% Al alloy are shown in Fig. 5. Although the correlation in site occupation is largely short range in nature as can be seen from Table 1, the strong, systematic departure from randomness is obvious.

It should be pointed out that the percentages of Cu atoms having the configurations plotted here are deceptively small. If it is assumed, for ease in computation, that the tetrahedra are isolated such that no Al atoms are counted more than once with this type unit, one finds that 83% of the Al atoms are in the $C17$ configuration for the B–S model data for a 16 at.% Al alloy. On the same basis, one finds 39, 20, and 5·5% of the Al in the tetrahedra for the 14·76, 13·56 and 9·13 at.% Al alloys respectively. If one extrapolates the experimental $C9$ curve to about 16 at.% Al, a similar calculation would indicate that all the Al is in this configuration. This is most certainly not the case, but it does demonstrate an important point. That is, at the higher concentrations there are more and more constraints on how the basic units can be packed together. It may well be significant in this sense that Gaudig (1975) and Gaudig & Warlimont (1978) have found long-period antiphase shift structures based on the $L1_2$, or Cu_3Au-type superlattice structure, in Cu–18·5 and Cu–19·5 at.% Al alloys after long-time annealing at 250 and 340°C.* If one were to extrapolate this behavior pattern to 25 at.% Al, one would find only the $C17$ and $C16$ configurations, in the ratio 2 to 1, in the $M = 1$ Cu_3Au-type antiphase-shift structure. In the various heat treatments investigated for the more concentrated alloy (14·76% Al), this ratio was found to be between $1{\cdot}5_1$ and $2{\cdot}2_5$.

While there is a certain obvious relationship in terms of the *first-nearest-neighbor* atomic configurations, it should be recalled that in this composition range we are not dealing with a highly ordered system. This can be concluded immediately from the fact that the order maxima are broad and diffuse. Furthermore, the local atomic arrangements are obviously complex, as indicated qualitatively by the structural detail in the diffuse diffraction diagram. Note, first of all, that the relatively simple $M = 1$ Cu_3Au-type antiphase-shift structure would result in sharp superlattice reflections at positions where even no diffuse maxima are observed experimentally. Periodic insertion of antiphase boundaries can generate a series of what are commonly called long-period superlattices. In either case, such behavior would indicate long-range correlations in site occupation due to pair interactions acting over substantial distances in the lattice.

In oversimplified terms, one could visualize the SRO as having arisen from a quasi-periodic array of close spaced, antiphase boundaries, or an equally valid general concept would appear to be that of locally ordered regions, with or without enrichment, embedded in a less ordered matrix. Direct, unambiguous evidence

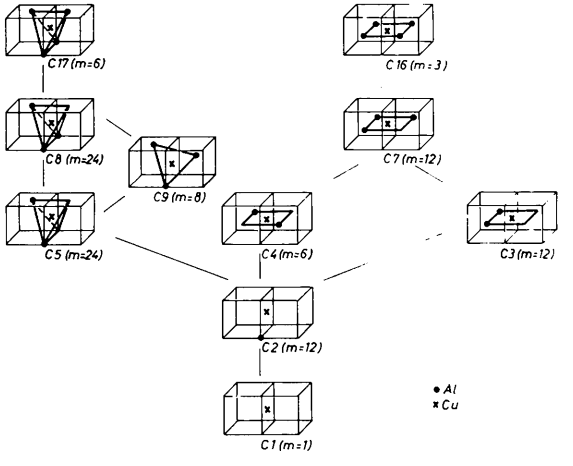

Fig. 4. The first-nearest-neighbor configurations of Al atoms (•) about Cu atoms (×) found in a Cu–14·76 at.% Al single crystal annealed 1 h at 650°C and quenched to room temperature. Two adjacent unit cells are outlined, and when no symbol is indicated it is to be understood that the lattice site is occupied by a Cu atom. The *Ci* are arbitrary designations (Clapp, 1971; Epperson, 1978) of the various possible configurations, and the *m*'s are the number of crystallographic equivalent variants of the indicated types.

* In alloys containing about 21 to 25 at.% Al, other long-period superlattices have been found by Bernard & Duval (1976).

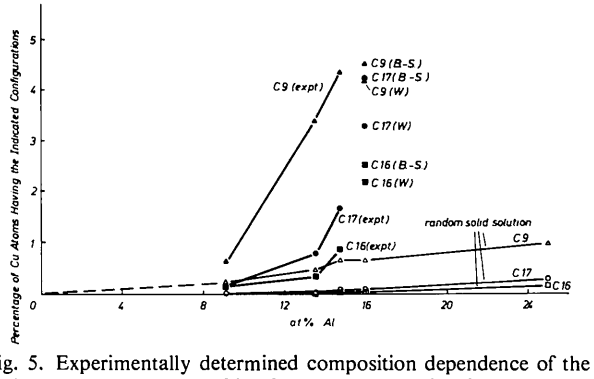

Fig. 5. Experimentally determined composition dependence of the three configurations, $C9$, $C16$, and $C17$, in Cu–Al alloys annealed 1580 h at 150°C compared with the corresponding concentrations found in random solid solutions. The points designated with B–S are values derived from the α_{lmn} from the random distribution of tetrahedra computed by Borie & Sparks (1964), and those designated by *W* are derived from the Williams (1974) analysis of the B–S two-dimensional data.

as to which, if either, is the proper characterization has not been easy to obtain for a weakly ordered system like this because of the very nature of SRO, *i.e.* its non-repeating character. The analytic techniques currently available do, however, permit one to determine that the *C*16 and *C*17 configurations are not always isolated in the short-range-ordered alloys investigated, as can be seen from the conditional probabilities given in Tables 5 and 6 for the first and second coordination shells, respectively, about the *C*17, *C*16, and *C*9 units. Note, for example, that for the Cu–14·76 at.% Al alloy there is a $2{\cdot}6_3\%$ chance of finding another tetrahedron centered on one of the eight remaining Cu atoms in the first coordination shell about the central Cu atom of a *C*17 unit. For the 13·56 at.% Al alloy, this correlation has decreased to $1{\cdot}8_5\%$, and no first-nearest-neighbor *C*17–*C*17 correlation is found for the 9·13 at.% Al alloy. Note also that in all three alloys there is a finite probability of finding a *C*16 on one of the eight remaining first *n*–*n* Cu atoms of a *C*17 unit. This is significant because such an extended atomic arrangement is an essential feature of the Cu_3Au-type antiphase-shift structures. That some ordered domains exist is further demonstrated by the conditional occupation probabilities for the second coordination shell as given in Table 6, especially the probability of finding a *C*17 unit about a *C*17 center in the two higher Al alloys. This extended ordered configuration is also to be found in the Cu_3Au-type antiphase-shift structures. The vast majority of the available sites in the first and second coordinate shells are not occupied in this way; thus the domain structure is not highly developed. No attempt will be made here to estimate the domain size; however, it appears as if a modest extension of the searching procedures used in this work would allow additional quantitative results to be extracted from the GC structures.

Even though, as we have seen, there is a marked resemblance between the local atomic configurations found in the three alloys investigated here and the series of LRO structures under discussion, it would be incorrect to assume that it is only a problem of kinetics preventing the development of LRO in these alloys. That the system is not approaching a long-range ordered state can be inferred from the behavior shown in Fig. 3. In order to test this point again, another 14·76% Al single crystal was quenched from 650°C. After annealing 172 h at 150°C, the peak unseparated diffuse intensity had decreased by 8%, confirming that there is a slight amount of disordering under these experimental conditions. This is further substantiated by measuring the isothermal 'recovery' of the electrical resistivity at 250°C after quenching a series of Cu–Al polycrystalline foils from 750 and 450°C. As shown in Fig. 6, those quenched from 750°C show a rapid, initial increase in resistivity, corresponding to some disordering, while those quenched from 450°C show just the opposite behavior, indicating an ordering process. Hence it can be concluded that short-range order is the equilibrium state in the composition range investigated.

Perhaps an additional word of caution should be injected at this point with respect to describing the SRO structure in terms of its antiphase nature. It would be fallacious to assume that the *local atomic arrangements* characteristic of an antiphase boundary must have arisen from impingement of ordered domains that nucleated at different sites. To the extent that the atomic order develops from randomly nucleated regions, this would be the logically expected behavior in a system in which long-range order evolves. Impingement may also occur in short-range-ordered systems, but it is not demanded, particularly in dilute, weakly ordered alloys. In this sense, it is considered especially meaningful that statistically significant numbers of the

Table 5. *Conditional probability of finding the indicated configurations on one of the remaining* Cu *atoms in the first coordination shell about the central* Cu *atom of configurations C*9, *C*16, *and C*17 *for* Cu–Al *alloys annealed* 1580 h *at* 150 °C *after quenching from* 650 °C

	About *C*17			About *C*16			About *C*9		
Ci	9·13 at. % Al	13·56 at. % Al	14·76 at. % Al	*Ci*	9·13 at. % Al	13·56 at. % Al	14·76 at. % Al	*Ci*	9·13 at. % Al	13·56 at. % Al	14·76 at. % Al
*C*3	0·3000	0·2708	0·2281	*C*3	0·6136	0·4271	0·3354	*C*2	0·4251	0·2350	0·1853
*C*5	0·3125	0·2593	0·2029	*C*7	0·1364	0·2656	0·2625	*C*3	0·0604	0·1168	0·1190
*C*7	0·1125	0·1296	0·1436	*C*8	0·2273	0·2552	0·3125	*C*4	0·0507	0·0826	0·0829
*C*8	0·2250	0·2037	0·2478	*C*16	0·0000	0·0104	0·0333	*C*5	0·3164	0·3272	0·2829
*C*9	0·0250	0·0903	0·1206	*C*17	0·0227	0·0365	0·0563	*C*6	0·0000	0·0019	0·0023
*C*10	0·0000	0·0000	0·0011	*C*18	0·0000	0·0052	0·0000	*C*7	0·0145	0·0214	0·0452
*C*11	0·0000	0·0023	0·0000					*C*8	0·1039	0·1491	0·1789
*C*12	0·0000	0·0023	0·0000					*C*9	0·0242	0·0446	0·0572
*C*16	0·0250	0·0162	0·0296					*C*11	0·0000	0·0005	0·0030
*C*17	0·0000	0·0185	0·0263					*C*12	0·0000	0·0009	0·0011
*C*18	0·0000	0·0046	0·0000					*C*17	0·0048	0·0185	0·0414
*C*19	0·0000	0·0023	0·0000					*C*18	0·0000	0·0005	0·0004
								*C*19	0·0000	0·0009	0·0004

tetrahedral and Cu_3Au-type ring configurations of Al about Cu atoms were found in the Cu–9·13 at.% Al alloy where there is vanishingly little domain character in the ordered structure. This would suggest that their formation is more fundamental and that the observed, ordered first-nearest-neighbor units reflect inherently stable spatial configurations of the atoms. The similarities of the ratios of the observed configuration concentrations (Tables 3 and 4) and that of the multiplicities (Fig. 4) is an indication that there is little difference in the formation energy for the DO_{22} structural unit ($C17$) and for the $L1_2$ unit ($C16$).

As was noted in a foregoing section, there has been previous structure-oriented experimental diffuse-scattering work by Houska & Averbach (1959) (H–A) on a powder sample and a more intensive two-dimensional investigation by Borie & Sparks (1964) on a single crystal. Borie & Sparks proposed that the SRO structure could be understood reasonably satisfactorily by assuming that the Al atoms are arranged tetrahedrally about Cu atoms and that the tetrahedra are distributed randomly, except that no Al–Al first nearest neighbors can result. This model was challenged by Gehlen & Cohen (1965) on the basis of a computer simulation of the H–A powder α_{lmn} in which no isolated tetrahedra were found. It was concluded that the most characteristic feature of the SRO structure was the occurrence of branched rods of second nearest-neighbor Al atoms and that the occasional existence of parallel or intersecting rods, at unit-cell distance, resulted in some plate-like ordered domains. The occurrence of so many second nearest-neighbor Al pairs is a reflection of the fact that α_{110} is at, or near, its theoretical lower limit (see Tables 1 and 2), and this is not unexpected because the atomic volume of Al is some 40% greater than that of Cu. The detailed information about the spatial arrangement is then contained in the succeeding α_{lmn}. It was pointed out by Clapp (1971) that the intersection of second-nearest-neighbor Al chains at unit-cell distance would produce the tetrahedral arrangement and the existence of parallel chains, again at unit-cell distance, would result in the Cu_3Au-type ring configuration.

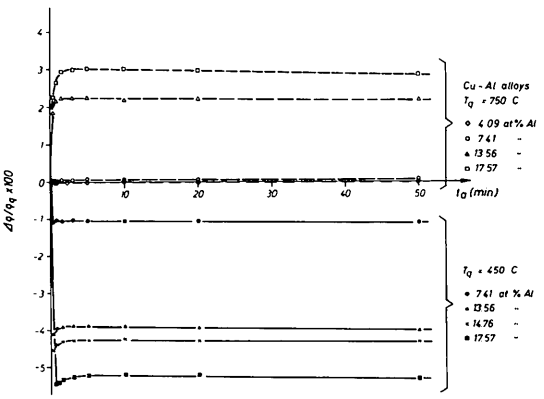

Fig. 6. Relative changes in the electrical resistivity during isothermal annealing at 250°C for a series of Cu–Al alloys quenched from 750 and 450°C. Each curve is normalized with the respective resistivity measured after quenching. All measurements were made at liquid-nitrogen temperature.

Two recent efforts have been made to re-analyse the B–S two-dimensional diffuse scattering data. Williams (1974) used a multiple regression analysis to obtain a set of α_{lmn} from which he simulated the SRO structure. It was concluded that the structure was heavily faulted Cu_3Au type, resulting in microdomains about 10 Å in diameter. A similar conclusion (microdomains about 17 Å in size) was arrrived at by Gaudig (1975) and Gaudig & Warlimont (1978) by fitting a two-dimensional antiphase-shift structure to the B–S experimental data. This antiphase *nature* of the structure was

Table 6. *Conditional probability of finding the indicated configurations on a site in the second coordination shell about the central* Cu *atom of configurations* $C9$, $C16$, *and* $C17$ *for* Cu–Al *alloys annealed* 1580 h *at* 150°C *after quenching from* 650 °C

	About $C17$				About $C16$				About $C9$		
Ci	9·13 at. % Al	13·56 at. % Al	14·76 at. % Al	Ci	9·13 at. % Al	13·56 at. % Al	14·76 at. % Al	Ci	9·13 at. % Al	13·56 at. % Al	14·76 at. % Al
$C2$	0·2833	0·1420	0·0717	$C1$	0·1060	0·0486	0·0235	$C2$	0·4130	0·1880	0·1469
$C3$	0·2333	0·1944	0·1600	$C2$	0·1060	0·1319	0·0986	$C3$	0·1014	0·1004	0·1003
$C4$	0·0667	0·0525	0·0433	$C3$	0·4394	0·2708	0·2958	$C4$	0·0616	0·0734	0·0768
$C5$	0·1500	0·2531	0·2533	$C4$	0·0000	0·0139	0·0070	$C5$	0·3043	0·3490	0·3445
$C6$	0·0000	0·0031	0·0000	$C5$	0·0152	0·0625	0·0469	$C6$	0·0000	0·0021	0·0006
$C7$	0·0833	0·1142	0·1117	$C6$	0·0000	0·0000	0·0023	$C7$	0·0326	0·0392	0·0328
$C8$	0·1833	0·1420	0·2417	$C7$	0·0758	0·2500	0·1854	$C8$	0·0726	0·1474	0·2063
$C9$	0·0000	0·0401	0·0467	$C8$	0·1970	0·1389	0·1948	$C9$	0·0145	0·0869	0·0669
$C10$	0·0000	0·0031	0·0033	$C10$	0·0000	0·0069	0·0023	$C10$	0·0000	0·0000	0·0019
$C16$	0·0000	0·0062	0·0217	$C16$	0·0000	0·0139	0·0376	$C11$	0·0000	0·0014	0·0043
$C17$	0·0000	0·0123	0·0433	$C17$	0·0000	0·0139	0·0305	$C12$	0·0000	0·0014	0·0006
$C18$	0·0000	0·0031	0·0017					$C17$	0·0000	0·0093	0·0173
$C19$	0·0000	0·0031	0·0017					$C19$	0·0000	0·0007	0·0000

recognized from the beginning (Borie & Sparks, 1964) as being the essence of the tetrahedron model.

The conclusion is inescapable that the various structural descriptions of the SRO cited in this section are essentially complementary, in contrast to the impression one is likely to get from some of the discussions presented. It would, thus, appear to be more meaningful to judge the various approaches on the basis of which is sufficiently general to characterize the SRO satisfactorily and to permit the changes which can be induced in the ordered state to be analyzed. That this complementarity is true can be demonstrated further by processing the α_{lmn} computed by Borie & Sparks from their tetrahedron model and those by Williams as the present data have been. In either case, a spectrum of nearest-neighbor configurations results that is qualitatively similar to those presented earlier from the present investigation, including the occurrence of the tetrahedra and Cu_3Au-type rings; however, there are significant quantitative differences as can be seen from Fig. 5. Because of the difference in alloy composition and in heat treatment, a rigorous comparison does not appear to be useful.

Based on the proven existence of the long-period superlattices in more concentrated Al alloys and their dependence on the electronic structure (Sato & Toth, 1963; Schubert, 1974) as well as the similarities in the SRO structure pointed out, a more detailed consideration of these α-phase Cu–Al alloys in terms of the interatomic potential (Moss, 1969; Wilkens, 1972; Semenovskaya, 1974; Morinaga, 1977) and the domain structure present would appear to be justified; that is, an extension of the work by Scattergood, Moss & Bever (1970). This is pointed out because, even though the raw data show the obvious characteristics of short-range order, there are additional indications that longer-range interactions are also involved. In particular, for the quenched Cu–14·76 at.% Al alloy, it was found that the SRO intensity in the $h_3 = 0$ plane computed from the modelled α_{lmn} produced the splitting in the diffraction pattern only if one included higher-order terms (to $l_{max} = m_{max} = n_{max} = 7$) in the summation indicated in the first term of equation (2). This information was, of course, originally contained in a complex way in the first six experimental α's; it is, in essence, the principle that the lower-order coefficients constrain the total configuration and hence largely determine the high-order correlations, which justifies one's creation and analysis of the GC structure. However, even with the same, or better, fitting to the first six α's, the computed diffraction patterns become less satisfactory with increasing annealing time at 250°C as the system approaches thermodynamic equilibrium. These observations are consistent with those by Williams (1974) and by Scattergood, Moss & Bever (1970) and seem to suggest strongly that longer-range forces are coming into play. Evidence to be presented elsewhere (Epperson, 1978) indicates that this will not seriously affect the first-nearest-neighbor configurations on which we have focused here, but it would surely be a more significant factor if one wished to characterize in detail the spatial configuration and/or distribution of ordered domains.

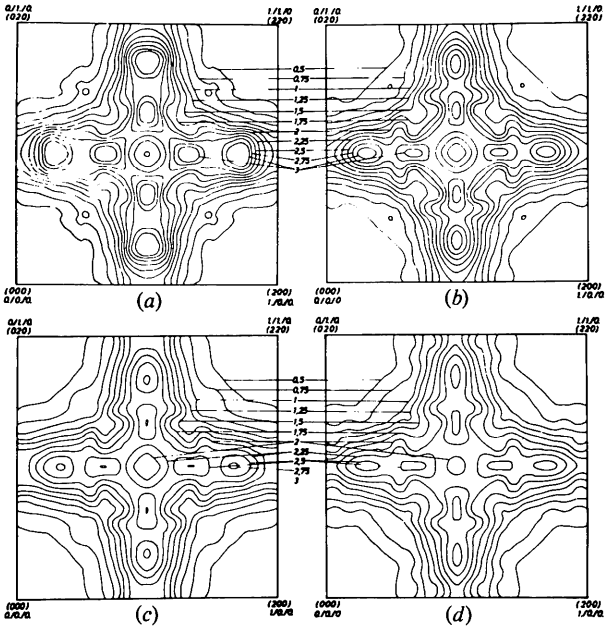

Fig. 7. Isointensity contour diagrams in the $h_3 = 0$ plane of reciprocal space for a Cu–14·76 at.% Al alloy: (*a*) 1 h at 650°C, quenched to room temperature. (*b*) 1 h at 650°C, q. to r.t., 2·5 min at 250°C, q. to r.t. (*c*) 1 h at 650°C q. to r.t., total of 20 min at 250°C, q. to r.t. (*d*) 1 h at 650, q. to r.t., total of 117 h at 250°C, q. to r.t. Shown is the component of diffuse scattering in Laue monotonic units due to the short-range order, *i.e.* after separation of the size effects. All intensity measurements were made at room temperature.

(*c*) *Isothermal annealing at* 250°C

It was shown earlier that annealing at low temperature following quenching from 600–800°C results

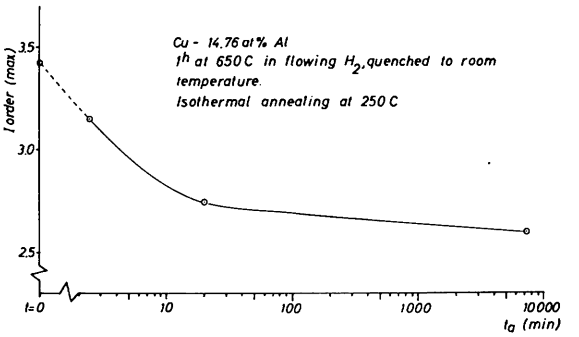

Fig. 8. Time dependence of the peak diffuse SRO intensity at $(h_1,h_2,h_3) \simeq (0{\cdot}5, 0{\cdot}133, 0{\cdot}0)$ *vs* annealing time at 250°C indicating the disordering process. These data are for the Cu–14·76 at.% Al single crystal quenched from 650°C. The intensity data are in Laue monotonic units.

in a disordering process. In Fig. 7 are presented a sequence of equal-intensity contour diagrams, in absolute Laue monotonic units, of the SRO component of the diffuse scattering from a Cu–14·76 at.% Al alloy annealed isothermally at 250°C following quenching from 650°C. That this represents a net disordering process is easier to see in Fig. 8, where the peak diffuse intensity is plotted against the annealing time. In view of the arguments to follow, it is worth emphasizing that these isothermal diffuse-scattering measurements were made on *one* single-crystal disc; it was quenched from 650°C and then annealed for additional time at 250°C and, of course, electropolished again before the next set of intensity measurements. Furthermore, the extrapolation to zero at the Bragg positions was done by computer, using a parabolic fit, in order to eliminate possible human bias. These procedures were adopted so that the observed changes in the scattered intensity could be analysed quantitatively with a minimum of uncertainty.

From the contour diagrams and tables of order coefficients (Table 2) alone, it is not possible to conclude much more than that the system is disordering during isothermal annealing at 250°C; however, a configurational analysis allows one to examine the mechanism involved more closely. The lower three curves in Fig. 9 show the time dependence of the $C9$, $C16$, and $C17$ configurations,* and a more complete listing of the configurations is given in Table 4.

The monotonic decrease with time in the $C16$ and $C17$ concentration was not unexpected; however, the small peak in the $C9$ concentration curve after 2·5 min annealing indicates the existence of a transition state in the disordering process. The following mechanism suggests itself.

With reference to the $C17$ chain in Fig. 4, the following pertinent reaction equations can be written:

$$C17 \rightleftharpoons C8 + Al \quad (7a)$$
$$C8 \rightleftharpoons C9 \quad (7b)$$
$$C8 \rightleftharpoons C5 + Al \quad (7c)$$
$$C9 \rightleftharpoons C5 + Al \quad (7d)$$
$$C5 \rightleftharpoons C2 + Al, \quad (7e)$$

where Al here means an Al atom that is no longer in the first coordination shell about the 'central' Cu atom of the reference configuration. As was indicated above, under the experimental conditions being considered the system is moving toward a state of thermodynamic equilibrium characterized by a lower degree of SRO. During the early stages of disordering, the break-up of the ordered configurations occurs in a slightly biased manner. The biased element would appear to be the jumping of an Al atom to the nearest-neighbor position such that configuration $C8$ transforms to $C9$. In the latter case, all the atoms are contained in a {111} type plane. While the present experiments do not allow one to determine if a faulted plane is involved, one suspects that to be the case. Stacking faults are surely present at

* The multiple points for a given annealing time result from having produced the GC structures completely anew by a different route, starting with the respective α_{lmn}, and from having searched them for the configurations. The creation of a GC structure is not an exact procedure in a short-range-ordered system, but the points shown here are an indication of the reproducibility that is attainable.

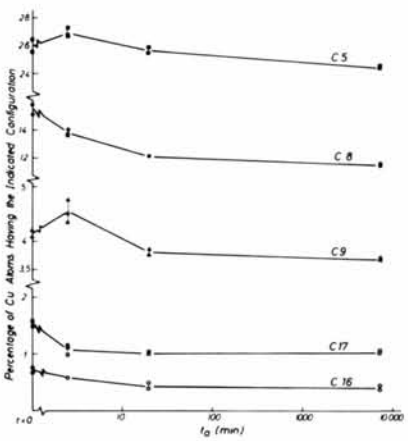

Fig. 9. Time dependence of the configurations $C5$, $C8$, $C9$, $C16$, and $C17$ in a Cu–14·76 at.% Al alloy quenched from 650°C and annealed isothermally at 250°C. The multiple points for a given annealing time are explained in the footnote.

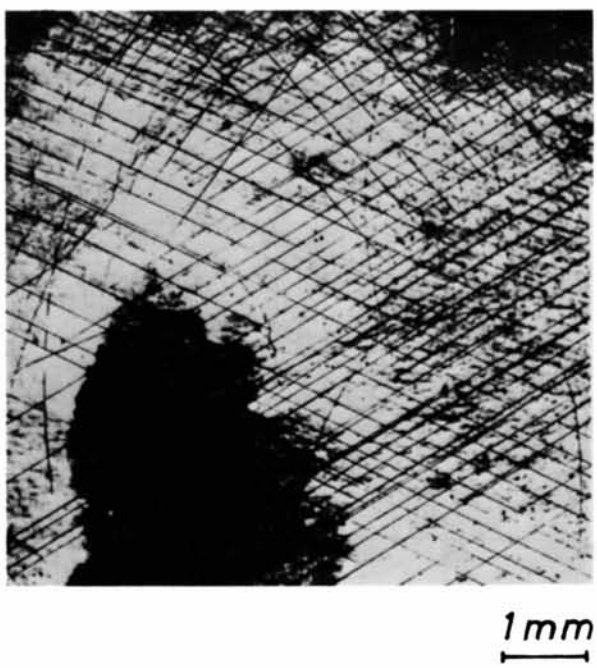

Fig. 10. Optical micrograph (12×) of the surface of a Cu–14·76 at.% Al single crystal quenched from 450°C into water at room temperature. Prior to heat treatment, the sample was electropolished, and the array of slip lines indicate that quenching stresses are sufficient to produce plastic deformation.

the beginning of this series of experiments. Quenching from 450°C is sufficient to produce substantial plastic deformation in these alloys, as illustrated by the array of slip lines on the surface of an electropolished Cu–14·76 at.% Al single crystal in Fig. 10. Similar results have been observed when electropolished single crystals were quenched from higher temperatures. It is also worth noting the behavior of configurations $C8$ and $C5$ in this range of annealing times. The percentage of $C8$'s drops less rapidly in the first 2·5 min than that of the tetrahedra (Fig. 9) due to the fact that $C8$'s are also being produced by reaction (7*a*). The $C5$ configuration is produced by reactions (7*c*) and (7*d*) and destroyed by reaction (7*e*). Furthermore, the occurrence of an isolated $C9$ triangle results in three other Cu atoms having the $C5$ configuration, and this is also contributing to the peak in the upper curve in Fig. 9. If the short-range-ordered structure consisted of isolated configurations, the process outlined here could be treated more exactly. In reality, the structure is rather complex, as we have seen, in the sense that it contains larger units which result from proper joining of the elementary nearest-neighbor configurations.

The transitory nature of the process described above is attributed to the fact that most of the stacking faults anneal out rapidly at 250°C. In addition to some measurements made during the course of this work, that faults anneal out rapidly at 250°C is known from the work by Mikkola & Cohen (1962), Mohan, Rao & Anantharaman (1965) and Saarinen (1968). A defect of the nature described above should affect the mechanical properties, and a peak in the hardness after short-time annealing at 250°C is observed as shown in Fig. 11 for a Cu–14·4 at.% Al alloy quenched from 650°C. Similar results have been reported on deformed alloys; by Chirikov (1972) on a Cu–17 at.% Al alloy annealed at 250°C and by Saarinen (1968) on a Cu–16 at.% Al alloy annealed at 300°C.

In essence, the reaction just described is what is commonly referred to as Suzuki locking. As was pointed out in the introductory section, there are sound theoretical grounds for expecting this reaction. One is fortunate in having a set of circumstances in which some stacking faults are produced by moderate quenching conditions, and, simultaneously, a non-equilibrium state of SRO results. Subsequently diffusion-controlled, local atomic rearrangements occur within a time–temperature interval in which at least some faults remain. By inference, the same type of reaction should result for these alloys at lower temperatures, as long as diffusion is possible. It should be emphasized that in this high-angle diffuse-scattering investigation, we are seeing a local atomic effect as opposed to a volume segregation of Al.

The contraction/expansion of stacking faults could conceivably be the source of one of the two processes noted by Veith, Trieb, Püschl & Aubauer (1975) in the resistivity changes induced by very small temperature excursions in the range from 220–245°C, although the dominant effect measured by Trieb, Siebinger & Aubauer (1973) appears to have been associated with changes in the degree of SRO.

(*d*) *Size effects*

It is apparent from a comparison of Figs. 2 and 7 for the total diffuse scattering and for the local-order component, respectively, that the atomic-displacement effects make a considerable contribution to the observed diffraction pattern. The size-effect coefficients (see equation 2) for the Cu–14·76 at.% Al alloy annealed 1580 h at 150°C are given in Table 7. Within the harmonic approximation of thermal oscillations, the first-order atomic displacements are purely static in nature. From Table 7 one sees that all the γ^{y}_{lmn} are quite small. Because there are essentially no Al–Al first-nearest-neighbor pairs for this case, it is possible to show that, as expected, the mean Cu–Cu distance is smaller and, consequently, that for the Al–Cu pairs is larger than the overall averaged nearest-neighbor inter-

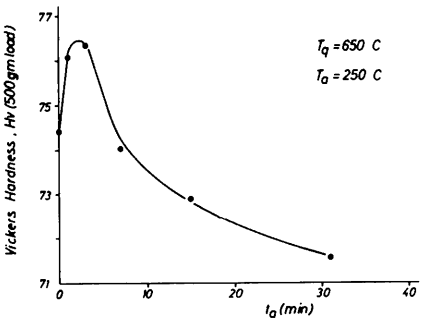

Fig. 11. Hardness *versus* annealing time at 250°C for a bulk, polycrystalline Cu–14·4 at.% Al alloy quenched from 650°C. The points shown are mean values determined from ten randomly placed indentations.

Table 7. *Size-effect coefficients for the* Cu–14·76 at. % Al *alloy annealed* 1580 h *at* 150 °C

i	*lmn*	γ^{y}_{lmn}	$\langle\delta^2\rangle^{y}_{lmn}$	$\langle\delta^2\rangle^{xy}_{lmn}$
0	000	0·000	−4·158	0·000
1	011	−0·045	−1·384	0·000
2	002	0·000	−1·053	0·000
3	112	−0·010	−0·754	−0·254
4	022	−0·019	−0·598	0·000
5	013	−0·004	−0·583	0·000
6	222	−0·031	−0·437	−0·519
7	123	−0·009	−0·353	−0·221
8	004	0·000	−0·383	0·000
9*a*	033	0·015	−0·189	0·000
9*b*	114	−0·003	−0·328	−0·053
10	024	−0·003	−0·247	0·000

atomic distance. The magnitude of the displacements estimated in this way is, however, unrealistic because the second-order size effects, *e.g.* the $\langle\delta^2\rangle^{y}_{lmn}$ and $\langle\delta^2\rangle^{xy}_{lmn}$ type series, are so large in comparison to the linear terms. Furthermore, the second-order size effects contain contributions from both static and thermal atomic displacements, and in the present experiments these contributions are not separable. Given the current state of the art, it is not possible to analyze the size effects in detail in a straightforward way as can be done for the short-range ordering of the atoms on the average lattice sites. This is unfortunate because there is certainly useful structural information embedded in these coefficients. The corresponding neutron diffuse-scattering experiment would be cleaner in that the scattering-factor (scattering-amplitude) ratios would be constant over the region of reciprocal space investigated, in contrast to the case for X-rays. For this system the ratios $f_{Cu}/(f_{Cu}-f_{Al})$ and $f_{Al}/(f_{Cu}-f_{Al})$ vary $\pm 5{\cdot}4$ and $\pm 11{\cdot}8\%$ respectively over the range of interest. On the other hand, it is clearly implicit in the foregoing discussion that even the quadratic approximation of the atomic displacements is being extended to its limit of validity because of the large displacements in this alloy system, and this would be true for the neutron experiments as well.

Concluding comments

The local-order structure in a series of α-phase Cu–Al alloys has been investigated in some detail in terms of the experimentally determined spectra of nearest-neighbor atomic configurations. This analysis was based on measurements of the scattered diffuse X-ray intensity in three dimensions in reciprocal space, determination of the Cowley–Warren order coefficients after separation of the atomic-displacement contributions, simulation of the real-space atomic structure, and classification of each atom in this structure according to the configuration of atoms in its first coordination shell. The searching routine requires no assumptions in addition to those already invoked either in the separation procedure or in the production of the GC structure; hence it is not necessary to assume *a priori* a specific model for the local atomic configurations.

The degree of short-range order is highly dependent on the thermal history. It was shown that for annealing temperatures above about 300–350 °C it is not possible to retain the high-temperature state of order in bulk single crystals by water quenching to room temperature. Two series of experiments were chosen for more intensive investigation; alloys containing 9·13, 13·56, and 14·76 at.% Al were quenched from 650 °C and annealed 1580 h at 150 °C in order to characterize the nature of the short-range order, and the disordering processes occurring when a Cu–14·76 at.% Al alloy is quenched from 650 °C and annealed isothermally at 250 °C were investigated.

The spectra of first-nearest-neighbor atomic configurations in the series of alloys annealed at 150 °C were found to be qualitatively similar. First-nearest-neighbor Al–Al pairs are excluded for this heat treatment. Ordered configurations designated as $C9$, $C16$, and $C17$ were prominent; these consist of three Al atoms in a close-packed plane about a Cu atom, four Al atoms in a ring in a cube plane about a Cu atom, and four Al atoms arranged tetrahedrally about a Cu atom, respectively. The $C17$ and $C16$ configurations are the basic structural units of the Cu_3Au-type antiphase-shift structures, and several long-period superlattice structures (or shift structures) have been found in recent years in alloys containing 18·5 at.% Al and more. It was demonstrated experimentally, however, that SRO is the equilibrium state for the alloys investigated, and this is probably true up to at least 16 at.% Al. There is clear evidence in the GC structure for the existence of some ordered domains in the higher-Al alloys, but it is considered equally fundamental that the ordered $C17$ and $C16$ configurations were found in the very weakly ordered Cu–9·13 at.% Al alloy. This is taken as experimental evidence that these configurations reflect inherently stable spatial arrangements of the atoms, as opposed to antiphase boundary effects.

When a Cu–14·76 at.% Al alloy is quenched from 650 °C and annealed isothermally at 250 °C, a net disordering process results. After an anneal of 2·5 min at 250 °C, a marked enhancement of the $C9$ configuration was found, and this is interpreted as evidence for the operation of the Suzuki mechanism. That is, there is an interaction of the solute Al atoms with the stacking faults. For quenching temperatures of at least 450 °C and above, the stresses generated by water quenching are sufficient to produce some plastic deformation. That the effect is transitory in nature is consistent with the fact that stacking faults anneal out rapidly at 250 °C. It was shown that the effect manifests itself also in the mechanical properties.

It is apparent that the theoretical basis is adequate and that the necessary manipulation of the experimental data can be handled routinely with currently available computing facilities. Thus investigations of the general type reported here, when combined with companion investigations of physical and mechanical properties, should yield valuable insight into the realtionships between the structural details and various material properties.

One of us (CO) wishes to acknowledge the financial support from the Deutsche Forschungsgemeinschaft. We are deeply indebted to Dr Cullie Sparks for loaning us the doubly bent monochromator. Even though we chose not to use them, we thank Professor E. A. Starke

Jr for giving us a battery of computer programs. We are grateful to Mr F. Eckstein for growing and cutting the single crystals and to Mrs E. Rücker for help in collecting the diffraction data. We also wish to acknowledge a useful discussion with Professor K. Schubert during the course of this work.

References

BERNARD, E. & DUVAL, P. (1976). *Phys. Status Solidi A*, **34**, 135–144.

BORIE, B. & SPARKS, C. J. JR (1964). *Acta Cryst.* **17**, 827–835.

BORIE, B. & SPARKS, C. J. JR (1971). *Acta Cryst.* A**27**, 198–201.

BROOKS, C. R. & STANSBURY, E. E. (1963). *Acta Metall.* **11**, 1303–1312.

CAHN, R. W. & DAVIES, R. G. (1960). *Philos. Mag.* **5**, 1119–1126.

CHIPMAN, D. R. (1956). *Rev. Sci. Instrum.* **27**, 164–165.

CHIRIKOV, N. V. (1972). *Phys. Met. Metallogr. (USSR)*, **33**(4), 161–163.

CLAPP, P. C. (1971). *Phys. Rev.* B**4**, 255–270.

COWLEY, J. M. (1950). *J. Appl. Phys.* **21**, 24–30.

CROMER, D. T. (1965). *Acta Cryst.* **18**, 17–23.

DOYLE, P. A. & TURNER, P. S. (1968). *Acta Cryst.* A**24**, 390–397.

EPPERSON, J. E. (1978). Submitted to *J. Appl. Cryst.*

EPPERSON, J. E., KOSTORZ, G., ORTIZ, C. & FÜRNROHR, P. (1978). In preparation.

FREEMAN, A. J. (1959*a*). *Acta Cryst.* **12**, 261–271.

FREEMAN, A. J. (1959*b*). *Acta Cryst.* **12**, 274–279.

GAUDIG, W. (1975). Doctoral Dissertation, Univ. Stuttgart (BRD).

GAUDIG, W. & WARLIMONT, H. (1969). *Z. Metallkd.* **60**, 488–498.

GAUDIG, W. & WARLIMONT, H. (1978). *Acta Metall.* In the press.

GEHLEN, P. C. & COHEN, J. B. (1965). *Phys. Rev.* **139**, A844–A855.

HASEGAWA, T., ASOU, K. & KARASHIMA, S. (1974). *Metall. Trans.* **5**, 933–938.

HOUSKA, C. R. & AVERBACH, B. L. (1959). *J. Appl. Phys.* **30**, 1525–1534.

HOWIE, A. & SWANN, P. R. (1961). *Philos. Mag.* **6**, 1215–1226.

IVERONOVA, V. I., KATSNELSON, A. A. & REVKEVICH, G. P. (1968). *Phys. Met. Metallogr. (USSR)*, **26**(6), 106–110.

MATSUO, S. & CLAREBROUGH, L. M. (1963). *Acta Metall.* **11**, 1195–1206.

MIKKOLA, D. E. & COHEN, J. B. (1962). *J. Appl. Phys.* **33**, 892–898.

MOHAN, A. P. R., RAO, P. R. & ANANTHARAMAN, T. R. (1965). *Trans. Indian Inst. Met.* pp. 173–176.

MORINAGA, M. (1977). *Acta Metall.* **25**, 957–962.

MOSS, S. C. (1969). *Phys. Rev. Lett.* **22**, 1108–1111.

NAKAJIMA, K., SLADE, J. J. & WEISSMANN, S. (1965). *Trans. Am. Soc. Met.* **58**, 14–29.

SAARINEN, A. V. A. (1968). *Acta Polytech. Scand. Chem. Ind. Metall. Ser.* **77**, 7–86.

SATO, H. & TOTH, R. S. (1965). *Alloying Behavior in Concentrated Solid Solutions*, edited by T. MASSALSKI, pp. 295–419. New York: Gordon and Breach.

SCATTERGOOD, R. O., MOSS, S. C. & BEVER, M. B. (1970). *Acta Metall.* **18**, 1087–1098.

SCHUBERT, K. (1974). *Acta Cryst.* B**30**, 193–204.

SEMENOVSKAYA, S. V. (1974). *Phys. Status Solidi B*, **64**, 291–303.

SUZUKI, H. (1952). *Sci. Rep. Tohoku Univ.* A**4**, 455–463.

TIBBALS, J. E. (1975). *J. Appl. Cryst.* **8**, 111–114.

TISONE, T. C., BRITTAIN, J. O. & MESHII, M. (1968). *Phys. Status Solidi*, **27**, 185–193.

TRIEB, L., SIEBINGER, K. & AUBAUER, H.-P. (1973). *Scripta Metall.* **7**, 245–251.

VEITH, G., TRIEB, L., PÜSCHL, W. & AUBAUER, H.-P. (1975). *Phys. Status Solidi A*, **27**, 59–67.

WARREN, B. E. (1954). *J. Appl. Phys.* **25**, 814–815.

WARREN, B. E. & MOZZI, R. L. (1966). *Acta Cryst.* **21**, 459–461.

WECHSLER, M. S. & KERNOHAN, R. H. (1958). *J. Phys. Chem. Solids*, **7**, 307–326.

WECHSLER, M. S. & KERNOHAN, R. H. (1959). *Acta Metall.* **7**, 599–607.

WILKINS, S. (1972). Doctoral Dissertation, Univ. of Melbourne, Australia.

WILLIAMS, R. O. (1974). *Metall. Trans.* **5**, 1843–1850.

Acta Cryst. (1978). A**34**, 681–683

A Fast-Converging Refinement of One-Dimensional Convolution Square Roots

BY HANS BRADACZEK AND PETER LUGER

Institut für Kristallographie der Freien Universität Berlin, Takustrasse 6, D-1000 Berlin 33, Federal Republic of Germany

(*Received 5 January* 1978; *accepted* 10 *April* 1978)

A fast-converging mathematical method for calculation of convolution square roots of one-dimensional functions has been developed. Application to one-dimensional periodic structure projections as well as to non-periodic structures is possible. Computer calculations of some examples are given.